Applied Water Science (2020) 10:131
https://doi.org/10.1007/s13201-020-01217-z

ORIGINAL ARTICLE

Kinetic equilibrium and thermodynamic analyses of As (V) removal from aqueous solution using iron-impregnated *Azadirachta indica* carbon

Ghazi Mohd Sawood[1] · **S. K. Gupta**[1]

Received: 28 January 2020 / Accepted: 28 April 2020 / Published online: 12 May 2020

Abstract
Arsenic emerges out as a potential threat to human health and vegetation in recent past. Therefore, the present study aimed at adsorption of As (V) from the aqueous solution using Fe-AIB and Fe-AIL (iron-impregnated activated carbon synthesized from the powder of bark and leaves of *Azadirachta indica* tree). The removal of As (V) by Fe-AIB and Fe-AIL was examined under different experimental conditions. The Fe-AIB showed up to 96% As (V) removal at pH of 6.0, and up to 90% removal was observed with Fe-AIL at pH 4.0. Although the kinetic data fit best in the pseudo-second-order model, there are various other processes like intraparticle diffusion, pore diffusion and film diffusion that controls the overall rate. Mechanistic frameworks related to the adsorption process were analysed using various isotherm models. Langmuir and Freundlich models clearly explain As (V) adsorption by Fe-AIB and Fe-AIL. Thermodynamic analysis reveals the spontaneous adsorption on Fe-AIB. Moreover, it also confers the endothermic nature of the adsorption process for both the adsorbents. The presence of co-existing ions like PO_4^{3-} and SiO_3^{2} negatively interfered the removal or arsenate uptake, whereas ions like SO_4^{2-} and NO_3^{-} do not significantly affect the adsorption process. Consistently greater than 90% As (V) removal up to few cycles for both the adsorbents was observed in regeneration studies. Significant reusability characteristics was possessed by both the spent adsorbents, which makes them potentially efficient for large-scale practical application with enhanced performance.

Keywords Adsorption · Arsenate · Adsorption isotherms · Fe-AIB · Fe-AIL

Introduction

Arsenic is a heavy metal and presents in abundance, primarily in environment and earth's crust. For living beings, arsenic is an essential element as it has wide use in pharmaceutical, agriculture and electronic industries, but toxicity caused by arsenic is an emerging issue (Hare et al. 2019). More than two hundred million people are affected by arsenic-contaminated groundwater worldwide, especially in Ganga–Brahmaputra and Indo-Gangetic plains. Recent research shows some new areas like Amazon basin also getting effected by As contamination (Upadhyay et al. 2019). Arsenic contamination of groundwater can be caused by natural sources, including weathering of minerals and rocks. Anthropogenic activities like processing of ore, extraction of metals, smelting, excessive use of fertilizer and pesticides cause transport and mobilization of As and highly induces its concentration in groundwater (Ranjan 2019). Arsenic exists in inorganic and organic form in an aqueous system. The organic form is of not much relevance as it easily gets detoxify through methylation. Inorganic As exists in rarely found oxidation states of −3 and 0 and very commonly found oxidation states of +3 and +5 in water system depending upon the redox conditions (Shankar et al. 2014). Pentavalent arsenic co-exists in the anionic form such as AsO_4^{3-}, $H_2AsO_4^{-}$ and is predominant species under oxidizing conditions (surface water). Trivalent arsenic exists in the non-anionic form such as $As(OH)_3$, AsO_2OH^{2-}, $As(OH)_4^{-}$, AsO_3^{3-} and AsO_2OH^{2-} and dominates under mild reducing conditions (groundwater) (Cullen and Reimer 1989; Singh and Pant 2004). Most of the As compounds do not possess any colour or smell; their presence in edible food or water cannot be detected easily and presents a serious threat to human health and environment (Mandal and Suzuki 2002).

✉ Ghazi Mohd Sawood
mohdsaud22@gmail.com

[1] Department of Chemical Engineering, Harcourt Butler Technical University, Kanpur, India

USEPA declared arsenic as Group A carcinogenic compound and considered as a severe potential threat to living being across the globe. Because of the notorious behaviour of As towards human health, the prescribed limit for As consumption by WHO is decreased to 10 ppb, which earlier was 50 ppb. There are various pathways through which As enters the human body, but ingestion of water and food is widespread (Smeester and Fry 2018). Mostly all organs of humans can be adversely affected by As toxicant. Basically, the effect on human health can be chronic or acute, which greatly depends on the amount of consumption and type of As (Ferreccio et al. 2013). Wide range of biochemical mechanism including mitosis activation, genotoxic damage induction, depletion of DNA fixing mechanism, signal cascades perturbation, etc., was proposed for arsenic as carcinogen (Tchounwou et al. 2019). Long-term consumption of As-contaminated water may result in As poising, also known as arsenicosis. Its pathological and clinical manifestations have been largely reported, and it comprises of pathologies related to skin, fibrosis of lungs and liver, atherosclerosis, loss of hearing and neurologic impairment in children (Tchounwou et al. 2015). In present work, the arsenic effect on human health has been distinguished as non-carcinogenic effects and carcinogenic effects (Table 1).

Due to easy oxidation of arsenite to arsenate, As (V) is in much more abundance in comparison with arsenite (Rango et al. 2013). Therefore, the present study aimed to remove As (V) from water. Due to the severity of arsenic threat, numerous arsenic removal technologies have been developed in recent past. A compact summary of them is given below (Tripathy and Raichur 2008; Nicomel et al. 2016; Asere et al. 2017).

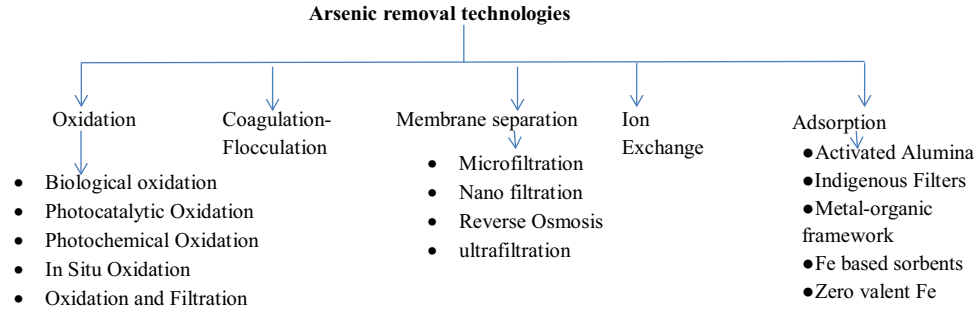

Table 1 Ways in which As effects human health

Non-carcinogenic effects	
Cardiovascular effect	Elevated blood pressure, hypertension and CVD were linked with chronic As consumption. Research shows areas exposed to prolonged As consumption are much prone to ischaemic heart diseases (IHD) (Tseng 2009)
Respiratory effects	Apart from lung cancer, there are many other effects on the respiratory system related to As poisoning. Research suggests the link of arsenicosis with chronic bronchitis. Moreover, vital capacity in children decreased by As (Smith et al. 2006)
Reproductive effect	The deleterious impact is shown by inorganic As on the reproductive system. Women affected by chronic As consumption shows positive trends towards premature delivery, complications in pregnancy and elevated fatal loss (Kwok et al. 2006)
Haematological effects	Haematological imbalance can be induced at higher rates with As exposure. Arsenic can be diabetogenic and can be a cause of type II diabetes (Tseng et al. 2000)
Neuropathic effects	Studies suggest that consumption of As in early age may affect the neurobehavioral system in the later phase of life. One of the most common issues related to the nervous system is peripheral neuropathy (Tsai et al. 2003)
Dermatologic effects	Keratosis, hypopigmentation and other types of skin lesions are common indicator of arsenicosis (Ahsan et al. 2000)
Effects on intellectual function and memory	A research on children in Mexico shows that with an increase in the concentration of As in urine, there is a decrement in verbal IQ, intellectual function and memory (Wasserman et al. 2004)
Carcinogenic effects	
Skin cancer	As the skin is one of the target organs in human by As, skin cancer induced by UV and intra-epidermal carcinomas can be greatly enhanced by inorganic As (Rossman et al. 2004)
Bladder cancer	Epidemiological studies show that the rate of bladder cancer and urinary system is positively linked to high As consumption, although there is an infrequent risk of bladder cancer in areas in which As exposure is less than 100 ppb (Baris et al. 2016)
Lung cancer	With increased As ingestion rates, mortality from this type of cancer increased. The risk of lung cancer increases with cigarette smoke as As and cigarette smoke are synergistic (Chen et al. 2004)
Liver cancer	There is huge risk of hepatocellular carcinoma and angiosarcoma, when arsenic exposure is combined with other genetic and environmental risk factors (Albores et al. 1996)

All techniques listed above, other than adsorption, require high fixed and running cost along with skilled human resources. Adsorption technique due to its low operational and fixed cost, easy operability, regeneration and less toxic sludge formation have the upper hand than other technologies, especially in developing regions (Boddu et al. 2008). Commercially available activated carbon is quite expensive, so in developing countries processes involving natural and locally available adsorbents were considered to be more promising due to their low investment and less impact on the environment (Asere et al. 2019). Being environment friendly, abundance and high efficiency, great interest is shown towards Fe-based adsorbents (Fe-based nanoparticles, Fe-based LDHs, zero-valent Fe, Fe-impregnated activated carbon, Fe-impregnated biomass and Fe-impregnated inorganic minerals) by the researchers in recent past for remediation of As (Hao et al. 2018).

The carbon obtained from the powdered bark and leaves of *Azadirachta indica* tree has proven to be excellent sorption materials for As (V) remediation. Because of abundance of these base materials, *Azadirachta indica* bark and leaves have drawn the attention of researchers in recent past for arsenate adsorption. At an optimum pH 5, maximum removal of arsenite, i.e. 90 per cent, was reported using ZnO nanoparticles doped into the *Azadirachta indica* leaves extract (Gnanasangeetha and SaralaThambavani 2015). By using the bark powder of *Azadirachta indica* at an optimum influent concentration 100 µg/L and 6pH, 79 per cent of arsenate was removed from the ground water (Choudhury et al. 2014). Also, at an initial concentration of 0–500 µg/L and Ph 6.5, maximum arsenite removal of 89 per cent was reported using the bark powder of *Azadirachta indica* (Roy et al. 2017) Moreover, *Azadirachta indica* powder in carbonized or uncarbonized form was frequently used earlier for the remediation of other contaminants including dyes (Srivastava and Rupainwar 2011), Cd(II) (Tiwari et al. 1999) Zn(II) (Bhattacharya et al. 2006) and Cr(VI) (Bhattacharya et al. 2008). Other plants bio-sorbents including Tamarix were also used for arsenate removal from the aqueous solution (Zhu et al. 2020).

These findings laid interest in exploring the probability for application of carbon obtained from the bark and leaves of *Azadirachta indica* for remediation of arsenate from aqueous solution. Also, there are numerous researches that have shown the compatibility of Fe oxides for arsenic removal, but due to high cost and fragile nature it cannot be used alone. Large number of iron-doped adsorbents were used earlier for arsenite remediation (Zhu et al. 2020; Lyu et al. 2020; Ali et al. 2020; Chen et al. 2020; Cui et al. 2019), but very less iron-impregnated adsorbents were used for arsenate removal (Verma et al. 2019; Zeng et al. 2020). In the present study, surface-modified bark and leaves of *Azadirachta indica* derived carbon were used for arsenate removal from the aqueous solution.

The present study aimed to develop low cost adsorbent derived from the impregnation of Fe on to the carbon derived from leaves (Fe-AIL) and bark (Fe-AIB) of *Azadirachta indica* tree and evaluation of kinetics, equilibrium and thermodynamics adsorption and kinetics studies of arsenate removal from aqueous solution, The novelty of the work is the performance evaluation of *Azadirachta indica* derived activated carbon, followed by its impregnation using iron metal, which was never been studied. The characterization of synthesized adsorbent was done through various analytical methods including scanning electron microscopy (SEM), energy-dispersive X-ray analysis (EDX), X-ray powder diffraction (XRD) and Brunauer–Emmett–Teller (BET) multipoint technique. The Fe-impregnated adsorbents have been used for the removal of As (V) at different operating conditions such as concentration, dose, time and pH after the treatment process; the testing of residual As (V) was done through ICP-MS.

Materials and method

Materials

Reagent-grade sodium arsenate ($NaHAsO_4{\cdot}7H_2O$), iron (II) chloride, hydrochloric acid, sodium hydroxide and sulphuric acid were procured from Merc India Ltd. Arsenate stock solution was prepared by dissolving 0.416 grams of sodium arsenate in deionized water and slowly rising the volume to 1 litre. 0.1 N NaOH or 0.1 N H_2SO_4 solution was used to control the pH. Deionized water was used to prepare the solutions for adsorption, synthesis and dilution.

Synthesis of Fe-AIB and Fe-AIL adsorbents

Activated carbon synthesized from the bark and leaves of *Azadirachta indica* tree was used in the present study. After pre-treatment, powdered bark and leaves are subject to sieving followed by carbonization in muffle furnace at 750 °C for 6 h and 3 h, respectively, with the circulation of N_2 gas. The activated carbon thus produced was subject to Fe impregnation using $Fecl_2$ salt solution. Series of thermochemical reaction takes place during the impregnation process. In the impregnation process, 50 g of activated carbon was added to a 0.5 M $Fecl_2$ solution and stirred at 70 °C for 24 h. NaOH was used to maintain the pH of suspension at 8 to increase the negative charge abundance. The filtrate was washed multiple times to remove the colloidal precipitates and iron salt attached to the surface of Fe-AIB or Fe-AIL (Kalaruban et al. 2019).The impregnation process using iron results in rearrangement of the pore structure of activated carbon and better affinity towards adsorbate (Shah et al. 2015).

Techniques used for characterization

Before the porosity and surface area measurement, degassing of AC and Fe-AC, at 300 °C for 18 h under vacuum, was done. The surface area was measured using Nitrogen adsorption isotherm at 77 °C by Brunauer–Emmett–Teller (BET) method. Average pore diameter and total pore volume were evaluated by Barrett–Joyner–Halenda method using Autosorb iQ. The surface morphology of samples and Fe distribution on activated carbon was studied using Carl Zeiss EVO 50 EDX coupled with scanning electron microscope operating at 20kv. XRD analysis for determining Fe species was done using Bruker D8 focus X-ray diffractometer having $\lambda = 1.5418$ Å and 2θ ranging between 5° and 80°.

Batch adsorption experiments

A series of Erlenmeyer flask (250 ml) containing 100 µg/L of 100 ml As (V) solution stirred in magnetic stirrer at a rate of 60 rpm was used to determine equilibrium time and optimum dose in the batch experiment. Volumetric flasks were used to prepare a standard solution. For investigating the effect of time of contact on overall removal, time of contact was varied from 15 to 75 min. By diluting the stock solution, concentrations ranging from 50 to 250 µg/L of As (V) were prepared. 0.1 M hydrochloric acid and 0.1 M sodium hydroxide were used to maintain the pH, and adsorbent dose was varied from 0.25 to 1.25 g while investigating the adsorption isotherm. To study the effect of temperature in a range 25–65 °C on uptake of As (V) by Fe-AIB or Fe-AIL, 1 g adsorbent was added to 100 ml of As(III) with initial concentration of 100 µg/L stirred at a rate of 60 rpm for various temperatures. Inductively coupled mass spectrophotometer (ICP-MS) was used to analyse the filtrate of solution to determine residue As (V). The quantity of adsorbed As (V) or the uptake capacity and percentage removal of arsenate was determined using Eqs. (1) and (2) (Yadav et al. 2014).

$$q_e\,(\mu g/g) = \frac{(c_i - c_e)V}{W} \tag{1}$$

and,

$$\text{Percentage As}\,(V)\,\text{removal} = \frac{c_i - c_e}{c_i} \times 100 \tag{2}$$

where c_i and c_e correspond to initial and equilibrium concentration of arsenate (µg/L), V is the volume of arsenate solution (L), and W represents the mass of adsorbent (gm).

Desorption and regeneration analysis

In desorption analysis, series of Erlenmeyer flask filled with 50 ml arsenate solution (100 µg/L) was used to treat 1 gm of the adsorbent. The adsorbent loaded with arsenate was filtered. To remove unadsorbed arsenate, the adsorbent subjected to multiple washing with deionized water. Then, the adsorbent was subject to hydroxide treatment at various concentrations, followed by filtration. The volume used for adsorption (V_a) was 50 ml, and that for desorption (V_d) was 25 ml, maintaining the V_d/V_a equals 0.5 (Chiban et al. 2016). The analysis of filtrate was done to evaluate the desorbed arsenate. Following equation was used to find out the amount of desorbed arsenate:

$$\text{Percent desorption} = \frac{\text{released arsenate (µg/L)}}{\text{initially arsenate adsorbed (µg/L)}} \times 100 \tag{3}$$

In regeneration studies, 50 ml arsenate solution (100 µg/L) was used to treat 1 gm of the adsorbent and allowed to filter after attaining the equilibrium. For time equal to adsorption period, the hydroxide treatment (20 ml NaOH) of adsorbent was done. Then, the filtration was done and filtrate was analysed for arsenate desorbed. Excess NaOH was removed by multiple washing of adsorbent. Again, the adsorbent was treated with 50 ml arsenate solution (100 µg/L).

Under identical conditions, the blank control test was performed. The amount of As (V) lost during the test was subtracted from the experimental results. All the experiments were performed in triplicate at room 25 °C (room temperature). The average experimental values were reported, and the standard deviation was represented using error bars. The relative experimental error was within ± 5% (Table 2).

Results and discussion

Characterization of Fe-AIB and Fe-AIL adsorbents

The BET surface area, pore width and pore volume of Fe-AIB and Fe-AIL are presented in Tables 3 and 4. The analysis shows decrement in surface area, pore width and pore volume after the Fe impregnation in both the samples. This decrease may be attributed to the blocking of some pores

Table 2 Physio-chemical properties of Fe-AIR

Analysis	Value	
	Fe-AIB	Fe-AIL
Moisture content (%)	10.95	13.81
pH_{zpc}	6.76	5.41
pH_{slurry}	6.23	5.19
Specific gravity (%)	0.227	0.208
Porosity	81	74
Particle size (µm)	227	251

Table 3 BET results of virgin AIB and Fe-AIB

	BET surface area (m^2/g)	Pore volume (cm^3/g)	Pore width (Å)
Virgin AIB	878.139	0.247	14.358
Fe-AIB	352.442	0.193	6.956

Table 4 BET results of virgin AIL and Fe-AIL

	BET surface area (m^2/g)	Pore volume (cm^3/g)	Pore width (Å)
Virgin AIL	359.732	0.169	6.135
Fe-AIL	192.116	0.092	2.974

The SEM micrographs of Fe-AIB and Fe-AIL reveal the surface morphology. It shows a very porous structure of Fe-AIB, as a large number of pores and grooves can be clearly seen (Fig. 1), which may have resulted in a large surface area of the material. The micrographs of Fe-AIL (Fig. 2) show fewer pores and heterogeneity as in comparison with the Fe-AIB. In some of the pores, the aggregates of Fe can be seen in the micrographs of both adsorbents.

The distribution of surface elements of Fe-AIB and Fe-AIL examined by EDAX is presented in Figs. 3 and 4, respectively. The EDAX analysis reveals that both the adsorbents mostly comprise of C, Cl and Fe, indicating mixed metal oxide composition. Cl and Fe are known to be good binding agents. Fe oxide is the dominant species of adsorbents as per the analysis of chemical composition.

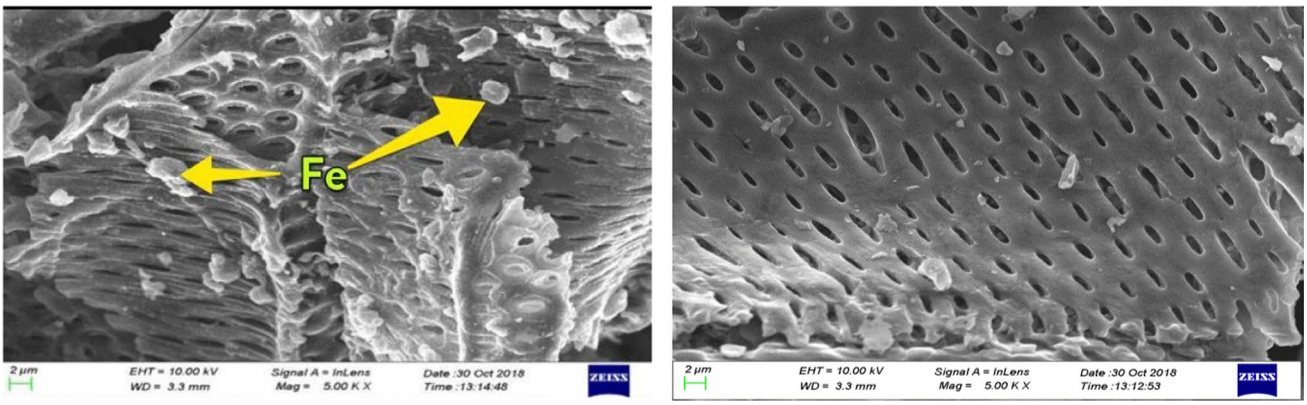

Fig. 1 SEM micrograph of Fe-AIB

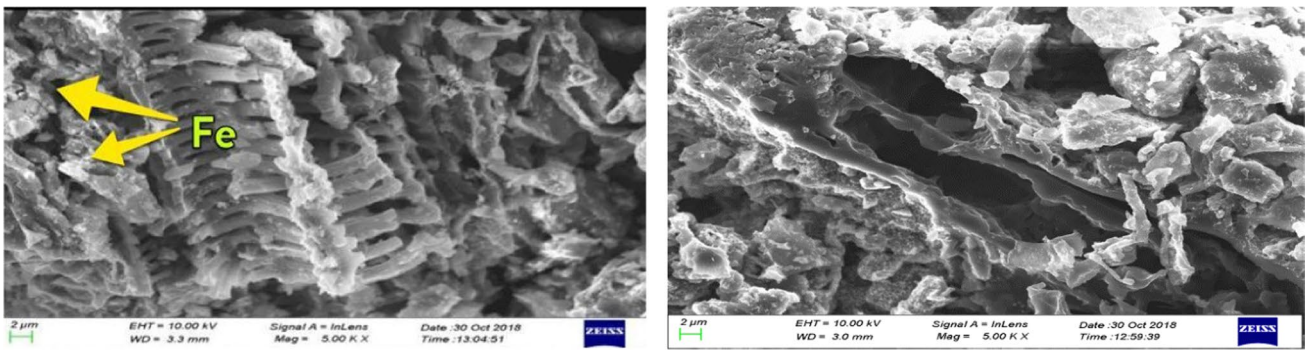

Fig. 2 SEM micrograph of Fe-AIL

in samples due to Fe coating. Same trends of decrement in surface area, pore width and pore volume due to Fe incorporation have also been reported earlier (Ryu et al. 2017). The average pore width of Fe-AIB was reported lying in the range of 5–15 Å, which reveals its microporous nature; on the other hand, Fe-AIL falls in the mesoporous category as the pore width of Fe-AIL is less than 5 Å.

The XRD pattern of prepared Fe-AIB and Fe-AIL is illustrated in Figs. 5 and 6. Fe-AIB and Fe-AIL show a peak at 2θ equal to 18° and 25°, respectively, which depicts the amorphous pattern of both the adsorbents. However, the peak in case of Fe-AIB is border and sharper as compared to the peak of Fe-AIL. This pattern of the peak is common in

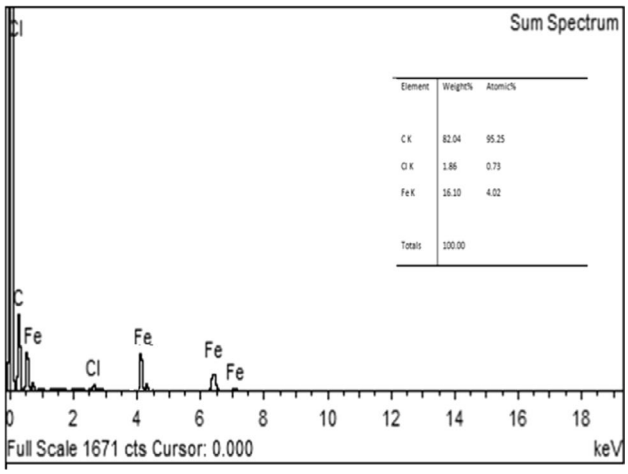

Fig. 3 EDX image and elemental composition of Fe-AIB

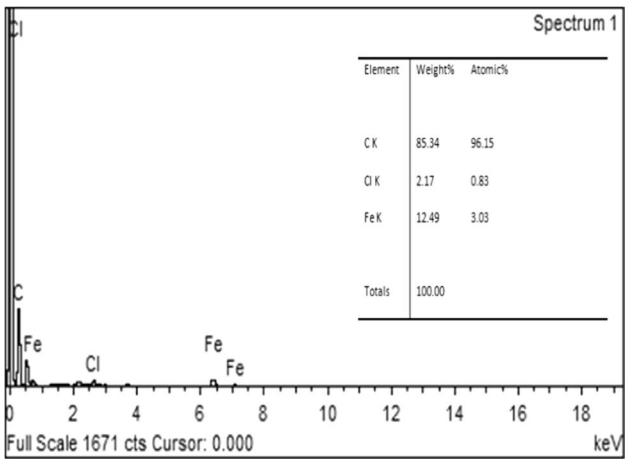

Fig. 4 EDX image and elemental composition Fe-AI

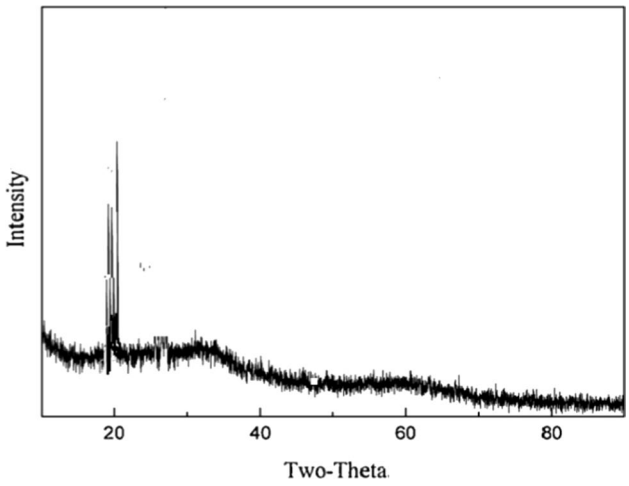

Fig. 5 XRD curve for Fe-AIB

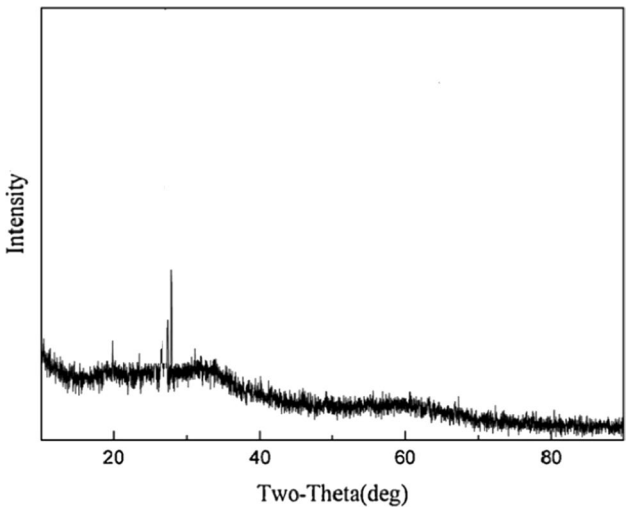

Fig. 6 XRD curve for Fe-AIL

amorphous material containing pyrolytic carbon with amorphous iron oxide and micro-graphitic structure (Naeem et al. 2016). XRD spectrum near to baseline subjects to amorphous nature of both adsorbents. From the literature, it can be concluded that amorphous nature of adsorbents is good for adsorption (Yakun et al. 2011).

The FTIR spectra of Fe-AIB and Fe-AIL recorded in the scale of 5000–450 cm^{-1}, before and after adsorption, are shown in Fig. 7. At 3206.5 cm^{-1} and 3504.2 cm^{-1} in Fe-AIB and Fe-AIL spectra (before adsorption), a characteristic peak appears which may correspond to O–H stretching or chemisorbed water content (Liu et al. 2014). In the As(V) adsorbed Fe-AIB and Fe-AIL, the peak shifted to 3241.7 cm^{-1} and 3432.1 cm^{-1}, respectively. A weedy adsorption band appears at 1520.7 cm^{-1} after adsorption of arsenate on Fe-AIB, which can be assigned to C=C stretching of the aromatic ring (Ravikovitch and Neimark 2006). A sharp peak before adsorption in Fe-AIB 1000.2 cm^{-1} at and small peak 1028.6 cm^{-1} at in Fe-AIL may result from C–OH stretching of COOH (Jadhav et al. 2015). After As (V) adsorption, the peak shifted to 1096.4 cm^{-1} in Fe-AIB and to 1152.3 cm^{-1} in Fe-AIL. A sharp peak at 892.4 cm^{-1} appears in Fe-AIB after adsorption may attribute to the interaction of metal and oxygen (Shah et al. 2015). No such peak is found in case of Fe-AIL.

Effect of initial arsenic concentration

The adsorptive behaviour of arsenate was analysed in the concentration range of 100–300 µg/L at pH 6.0, adsorbent dose of 1 g, stirring rate of 60 rpm and 25 °C temperature for the time of contact of 1 h, as shown in Fig. 8. The trend shows decrement in percentage removal of As (V) on

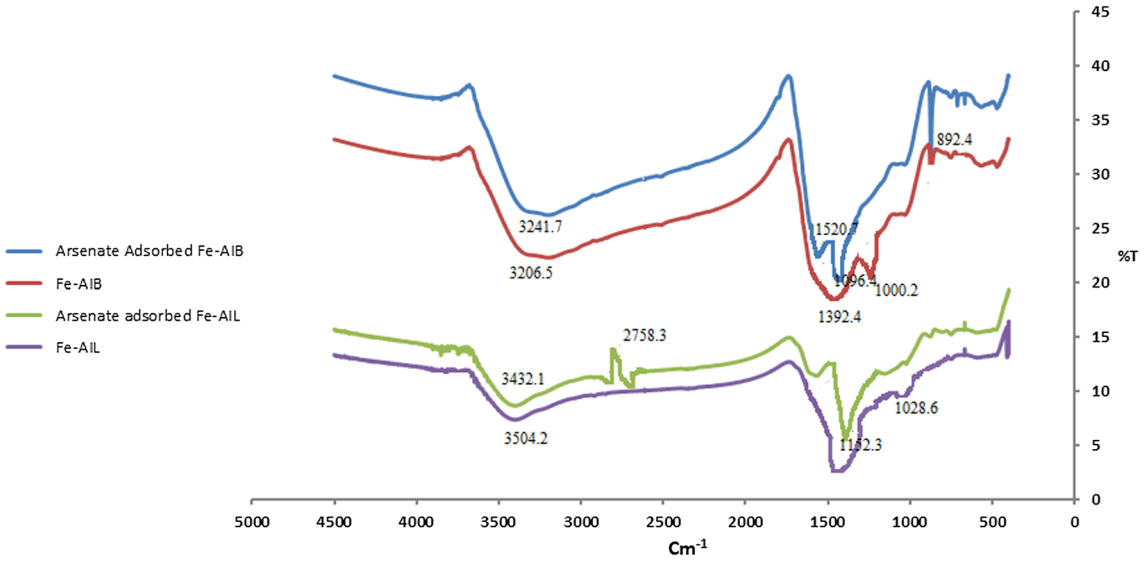

Fig. 7 FTIR spectra of Fe-AIB and Fe-AIL before and after adsorption

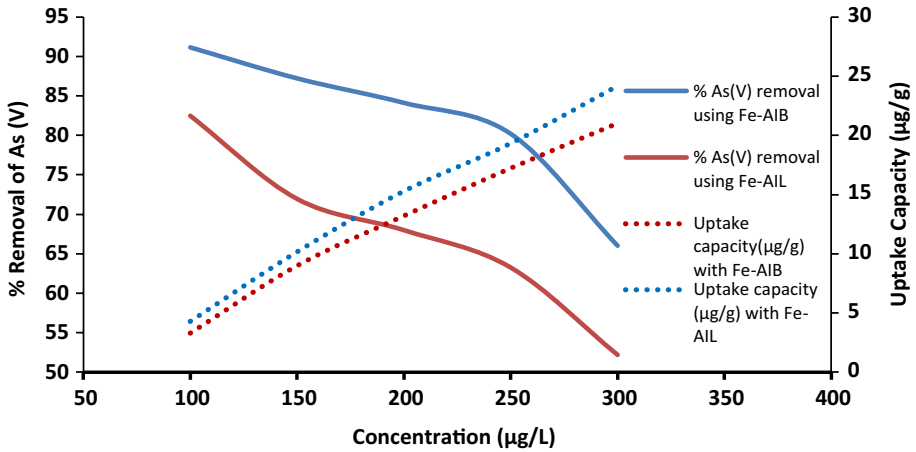

Fig. 8 Effect of initial arsenic concentration on adsorption of As (V) by Fe-AIB and Fe-AIL

Fe-AIB and Fe-AIL with increase in initial As (V) concentration. This decrement may result from the saturation of active adsorption sites.

The ratio of ion and adsorbent increases which saturates the higher energy sites, and efficiency of adsorption gets decreased (Mondal et al. 2012). But with increase in As (V) concentration, the quantity of As (V) adsorbed per unit mass of Fe-AIB and Fe-AIL increases. This increase may be attributed to lowering in resistance to the uptake of As (V) with increase in concentration (Bhaumik et al. 2011).

Effect of adsorbent dose

To attain the maximum capacity of adsorption of Fe-AIB and Fe-AIL and hence the maximum percentage of As (V) removal from the water phase, the adsorbent dose varied from 0.25 to 1.25 g/L. Further addition from 1 g/L in case of Fe-AIB and 0.75 g/L in case of Fe-AIL does not reduce the As (V) residual concentration. These findings are shown in Fig. 9. This increase in As (V) removal percentage with increase in dose may be due to enhanced surface area and availability of more adsorption sites (Božić et al. 2009). The saturation in removal efficiency of Fe-AIB after 1.00 g/L and of Fe-AIR after 0.75 g/L may be due to attainment of maximum adsorption. Hence, the number of ions remains constant even with further increase in adsorbent dose (Thapa and Pokhrel 2012).

Effect of time of contact

The impact of contact time on adsorption of As (V) using Fe-AIB and Fe-AIL was studied in the time span of 15–75 min

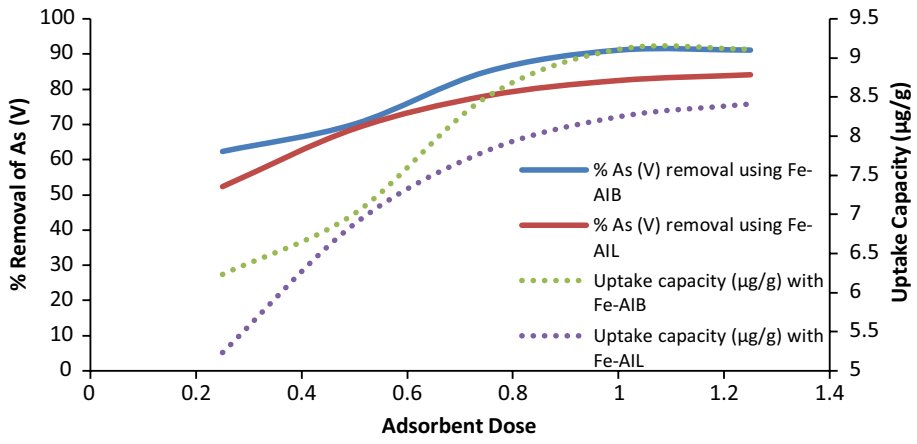

Fig. 9 Effect of adsorbent dose on adsorption of As (V) by Fe-AIB and Fe-AIL

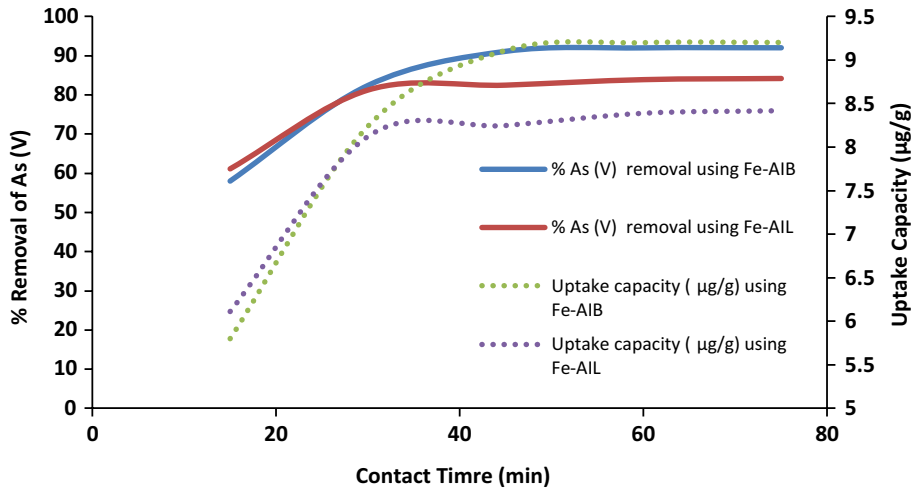

Fig. 10 Effect of contact time on adsorption of As (V) by Fe-AIB and Fe-AIL

at pH 6.0, and 1.0 g dose is shown in Fig. 10. The per cent As (V) ion removal as a function of contact time depicts biphasic nature on the surface of both the adsorbents with a quick uptake up to 45 min for Fe-AIB and 30 min for Fe-AIL and gradually attains equilibrium after that. After that, no significant change in per cent As (V) removal was observed. The availability of a large number of binding sites on the surface of adsorbent at an initial phase may result in quick adsorption. Due to repulsive forces between As (V) molecules on the surface of adsorbent and bulk phase in the later phase, the occupancy of left out vacant sites became difficult (Rajesh 2010).

Effect of pH

At an optimum concentration of 100 µg/L, the uptake capacity and per cent removal of As (V) as a function of pH by Fe-AIB and Fe-AIL are shown in Fig. 11. For Fe-AIB, the optimum per cent removal obtained as 93.997 (9.337 µg/g) was attained at 6.0 pH. $HAsO_4^{2-}$ and $H_2AsO_4^-$ were the predominant species in the pH range of 2–10. In the pH spectrum of 4–6, the arsenate species exist mainly as $H_2AsO_4^-$ and $HAsO_4^{2-}$ in pH range of 8–10. Both the species co-exist in the 6–8 pH range. At optimum pH, the probable mechanism is adsorption of $HAsO_4^{2-}$(anionic species) on to positively charged adsorption sites through the bonding with R-OH group present on the Fe-AIB surface (Kumari et al. 2005). The decrement in removal efficiency at high pH can be attributed to dominancy of density of OH^- ions, which results in their competition with anionic arsenate species. Moreover, at alkaline pH, R-OH, R-COOH and R–CO–NR groups of Fe-AIB are negatively charged and result in repulsive force between the anionic arsenate species and the adsorbent (Sarı and Tuzen 2010). For Fe-AIL, the optimum removal of 88.698% was obtained at 4.0 pH. This can be attributed to the fact that arsenate species are efficiently adsorbed at acidic conditions. Adsorption of As (V) by Fe-AIL is supposed to be performed by as anion exchange along with physiochemical adsorption. Under acidic conditions, the surface of adsorbent is positively charged, which get balanced by their escort anions (Ansari and Sadegh 2007).

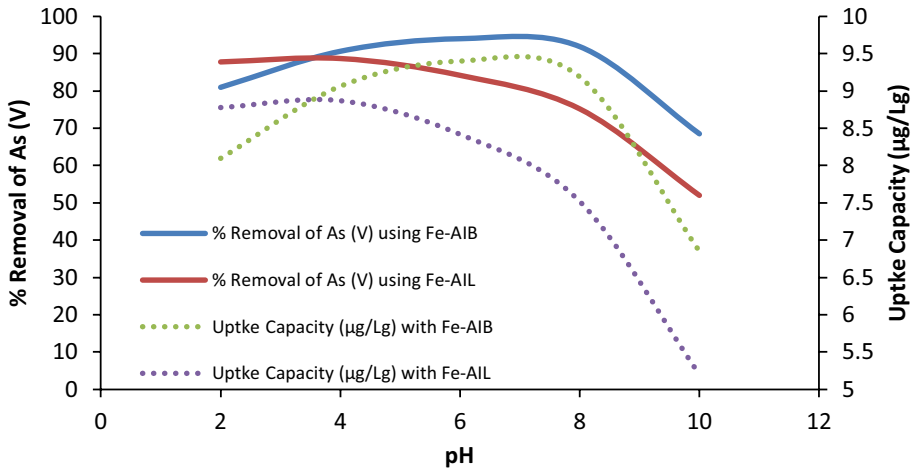

Fig. 11 Effect of pH on adsorption of As (V) by Fe-AIB and Fe-AIL

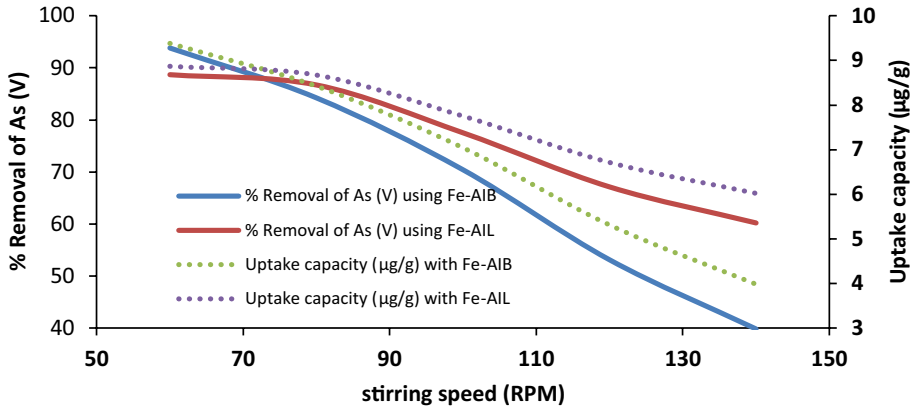

Fig. 12 Effect of stirring rate on adsorption of As (V) by Fe-AIB and Fe-AIL

Effect of stirring rate

The effect of different rates of stirring varying from 60 and 120 rpm at optimum conditions was analysed for Fe-AIB and Fe-AIL and is presented in Fig. 12. For both the adsorbents, it was observed that the removal efficiency decreases with increase in stirring rate. This decreasing trend of removal efficiency can be due to the fact that less time is available for the interaction of arsenate ions and surface of the adsorbent for interaction at high agitation speeds which also can separate the ions that are loosely bounded (Roy et al. 2014). Removal percentage of As (V) drastically decreases with increase in stirring rate. This decrease in removal percentage can be attributed to the fact that less time of contact available for adsorbent and adsorbate and hence results in reduced adsorption when the rate of stirring increases.

Effect of temperature

The impact of temperature on the removal of As (V) by Fe-AIB and Fe-AIL at various temperatures ranges from 303 to 325 K. Figure 13 presents that removal percentage using Fe-AIB increases from 91.525 to 94.614% when temperature changes from 301 to 313 K and then decreased. The same trend was observed using Fe-AIL, where removal percentage changes from 88.175 to 90.432% when temperature changes from 303 to 308 K and declines after that. This may be attributed to the fact that both the adsorbents are losing their adsorption capacity at elevated temperatures by means of denaturation. Also arsenate ions (solute) move with high rates at elevated temperature and time available for their interaction with active sites of adsorbent decreases (Kanwal et al. 2012).

Adsorption kinetics analysis

The physicochemical study of adsorption kinetics is significant as it provides valuable information about reaction mechanism involved and pathways of reaction. Moreover, it also provides the uptake rate of solute, which describes the residence time of solute on the surface of the adsorbent. In the current study, the As (V) adsorption kinetics and mechanism of adsorption on the prepared adsorbents were evaluated at various temperatures. Pseudo-first-order, Pseudo-second-order, Elovich equation, Bangham model and intraparticle diffusion models were used to evaluate

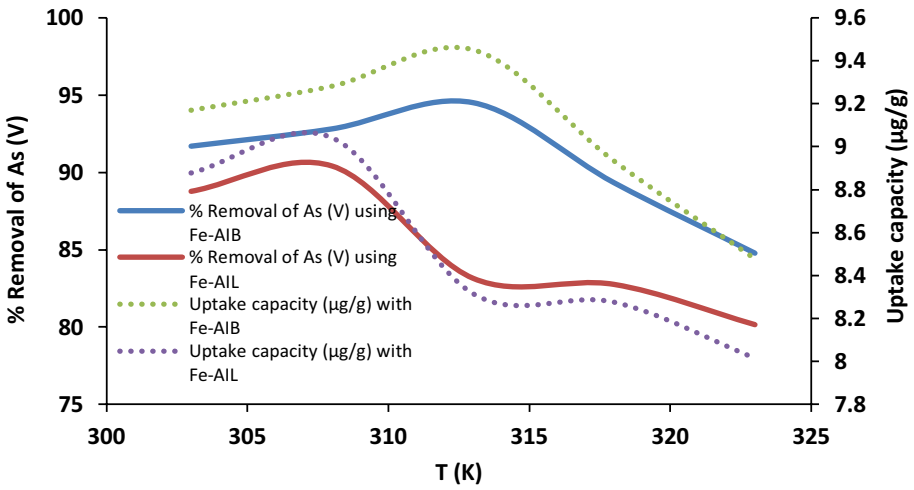

Fig. 13 Effect of temperature on adsorption of As (V) by Fe-AIB and Fe-AIL

Table 5 Kinetic parameters for adsorption of arsenic by Fe-AIB and Fe-AIL

Kinetic model	Parameters	Fe-AIB		Fe-AIL	
		Values	R^2	Values	R^2
Pseudo first order	$q_{e,\exp}$ (µg/g)	10.9917	0.915	9.4702	0.821
	q_e (µg/g)	5.8159		1.3452	
	K_1 (g/µg-min)	0.0017		0.0004	
Pseudo second order	$q_{e,\exp}$ (µg/g)	10.9917	0.997	9.4702	0.991
	q_e (µg/g)	11.7708		9.1313	
	K_2 (g/µg-min)	0.0074		0.0031	
Intraparticle diffusion	k_{pi} (µg/g $\text{min}^{\circ.5}$)	0.7642	0.844	0.6049	0.865
	C	3.4874		4.0144	
Elovich model	α (µg g^{-1} min^{-1})	12.1553	0.959	1.87552	0.920
	β	0.4288		0.5406	
Bangham kinetic model	k_r (µg/g-min)	9.6421	0.92	3.1479	0.891
	m	3.1968		4.0069	

the obtained data. Parameters of the five models are listed in Table 5. The R^2 (coefficients of determination) values determine the goodness-to-fit model. Relatively higher values of coefficients of determination show that the model well describes the kinetics of As (V) adsorption by the adsorbents.

The Lagergren first-order equation assumes that the overall rate of adsorption is proportional to the difference in concentrations at saturation and the cumulative quantity of solute uptake. The pseudo-first-order rate equation is expressed as Eq. (4) (Depci et al. 2012)

$$\text{Log}\{(q_e) - (q_t)\} = \text{Log}\{q_e\} - \frac{k_1}{2.303}t \tag{4}$$

where the quantity of As (V) adsorbed after time t and at equilibrium (µg/g) is denoted by q_t and q_e, respectively. k_1 is the rate constant for the first-order model. Lower values of R^2 and vast gap between the calculated and experimental values of maximum solute adsorbed (Table 6) show that Pseudo-firs- order model is unsuitable for explaining the mechanism for the As (V) uptake by and Fe-AIL.

Ho and Mckay second-order model assumes that sharing of electrons through chemisorption controls the rate of adsorption. It deals more with mechanism of chemical reaction. The pseudo-second–order kinetic equation is as Eq. (5) (Bayramoglu et al. 2009)

$$\frac{t}{(q_t)} = \frac{1}{(k_2)(q_e)^2} + \frac{t}{(q_e)} \tag{5}$$

where k_2 is the rate constant for the second-order model, q_t is the arsenate adsorbed after time t, and q_e is the arsenate adsorbed on Fe-AIB and Fe-AIL at equilibrium. The slope of plot t/q_t versus t would yield q_e (adsorption capacity at equilibrium). From Table 6, it can be seen that the difference between q_e and $q_{e,\exp}$ values is very less along with good R^2

Table 6 Isotherm data for adsorption of arsenate by Fe-AIB and Fe-AIL

Adsorption isotherm	Parameters	Fe-AIB		Fe-AIB	
		Values	R^2	Values	R^2
Langmuir isotherm	q_{max} (µg/g)	36.9636	0.9937	29.1812	0.9989
	K_L (L/µg)	0.0516		0.1145	
	R_L	0.1623		0.0803	
Freundlich isotherm	K_F (µg/g)	2.1712	0.9899	1.0362	0.9912
	n	1.6130		1.2786	
Temkin isotherm	A_T (L/µg)	0.7203	0.983	0.0453	0.970
	b_T (J/mol)	324.2599		79.4315	
	B	8.7199		5.7896	
D–R isotherm	q_{max} (µg/g)	21.9289	0.9037	19.1885	0.9169
	E (J/mol)	45.342		6.3845	

value, so it can be concluded that second-order model can very well approximate adsorption reaction mechanism.

Weber–Morris intraparticle diffusion graph is used to evaluate the mechanism involved in the adsorption process. The Weber–Morris intraparticle model is given by eq. (6) (Bazarafshan 2017)

$$q_t = k_{pi} t^{0.5} + C \tag{6}$$

where q_t is arsenic adsorbed on Fe-AIB and Fe-AIL after time t, k_{pi} is the intraparticle diffusion rate constant, and constant C gives the thickness of the boundary layer. A low value of C implies less effect of the boundary layer on the process of adsorption. q_t versus $t^{0.5}$ correspond to multi-linearity plot having two adsorption stages. First linear portion represents mass transfer at faster rates through film diffusion, and the second portion corresponds to uptake of As (V) through intraparticle diffusion. It is conferred that intraparticle diffusion and film diffusion takes place simultaneously as the straight line is not passing through origin (Nandi et al. 2009). The values of k_{pi}, C and R^2 values from the table infer that during adsorption of As (V) on Fe-AIB and Fe-AIL, one of the rate controlling steps is intraparticle diffusion.

Elovich model explains the phenomenon of chemisorption with negligible desorption. This model assumes that adsorption rate decreases as the surface coverage increases with time. Elovich model is given by Eq. (7) (Juang and Chen 1997)

$$\frac{dq_t}{dt} = \alpha \exp(-\beta q_t) \tag{7}$$

where α (mg g^{-1} min^{-1}) a is the rate constant for initial adsorption, and β is the rate constant for desorption. The simplified form of Eq. (7) can be written as:

$$q_t = \frac{\ln(\alpha\beta)}{\beta} + \frac{\ln(t)}{\beta} \tag{8}$$

q_t versus t yield a plot in the present study for both the adsorbents indicate switching from one active site to another site having different kinetics of the reaction. For the case of Fe-AIB, Elovich plot can be subdivided into two stages. In the first stage, the adsorption takes place at a faster rate on to the adsorbent surface, and in a later stage, the adsorption takes place in the inner surface may be in micropore (Chien and Clayton 1980). No such trend was observed in the Elovich plot of Fe-AIB, suggesting that a major portion of the adsorption process takes place on the outer surface of Fe-AIL.

Bangham kinetic model was used to investigate the role of pore diffusivity in the present study. The linear form of Bangham kinetic equation will be given by Eq. (9) (El Saliby et al. 2013)

$$q_t = (k_r) t^{1/m} \tag{9}$$

where q_t is the quantity (µg/g) of As (V) adsorbed at time t (min), k_r is the rate constant for As (V) adsorption, and factor 1/m represents the intensity of adsorption. From the Bangham plot for Fe-AIB, the value of K_r comes out be very close to the obtained value of adsorbed amount ($q_{e,exp}$) and linear nature of obtained curve suggests pore diffusion plays an important role in the adsorption of As (V) (Taştan et al. 2012). For Fe-AIL, the straight line obtained is not very linear, suggesting its deviation from Bangham model. It can be observed that the overall reaction rate cannot be controlled by pore diffusion alone, but also by film diffusion and intraparticle diffusion.

Adsorption isotherms models

Adsorption isotherms are mathematical models used to predict adsorbate distribution among the solid–liquid phase, and obtained data are helpful in evaluating the mechanism of adsorption. There are numerous models used in the literature to enumerate experimental findings of adsorption isotherm. The Langmuir (LM), Freundlich (FM), Temkin (TM) and Dubinin–Radushkevich models (D–RM) are the most frequently used models. In the current study, these four models were used to explain the relationship among the adsorbed quantity of As (V) on Fe-AIB and Fe-AIL with its concentration at equilibrium.

LM Isotherm

The obtained data were fitted to LM adsorption isotherm at equilibrium by assuming adsorbent having identical finite number of active sites upon which monolayer adsorption

taking place. Following equation in linear is used to express isotherm (Langmuir 1918):

$$\frac{1}{q_e} = \frac{1}{q_{\max} K_{\mathrm{LC}_e}} + \frac{1}{q_{\max}} \tag{10}$$

where q_e is the As (V) concentration at equilibrium on the Fe-AIB and Fe-AIL (µg/g), Ce is the equilibrium arsenate concentration in the solution (µg/l), $q_{\max}$ (µg/g) is the adsorption capacity (maximum) of the adsorbent, and K_{L}(l/µg) is the Langmuir constant and is associated with the free energy of adsorption. The value of all these parameters obtained from the plot of $1/q_e$ versus $1/c_{\mathrm{e}}$ is presented in Table 6. Higher values of R^2 (above 0.99) for both the adsorbents represent a good fit of LM to adsorption of As (V) on the adsorbents. Separation factor (R_{L}) is one of the important parameters of LM isotherm which tells whether the adsorption is favourable or not and mathematically can be expressed as given in Eq. (11)

$$R_{\mathrm{L}} = \frac{1}{1 + K_l C_i} \tag{11}$$

R_{L} values lying in between 0 and 1 correspond to favourable adsorption (Bulut et al. 2007). In the present study, the values of R_{L} obtained from both the adsorbents are presented in Table 6. It can be seen that the R_{L} value for Fe-AIB is 0.1623 and for Fe-AIL is 0.0803, indicating the favourable adsorption.

FM Isotherm

Then, the obtained data were fitted to FM adsorption isotherm, which assumes that free energy of adsorption is heterogeneous in nature and varies with the surface coverage (Freundlich 1906). Mathematical expression of FM isotherm can be give by Eq. (12)

$$\log\, q_e = \log\, K_{\mathrm{F}} + \frac{1}{n} \log\, C_e \tag{12}$$

where K_{F} and n are FM isotherm constant and can be evaluated from the linear plot of log q_e versus log c_{e}. n indicates how favourable adsorption process is. $1/n$ values in the range 0–1 are measure of intensity of adsorption and heterogeneity of surface; heterogeneity increases as the value approaches 0. 1/n value below 1 corresponds to normal LM isotherm. The values of FM isotherm constants and R^2 for Fe-AIB and Fe-AIL are also presented in Table 6. The numerical value of n for Fe-AIB is 1.6130 and for Fe-AIL is 1.2786, indicating that As (V) ions are adsorbed favourably. FM model does have good agreement with experimental data as the values of R^2 are high for both the adsorbent. The capacity of the microparticle to remove As (V) confers by these findings.

TM Isotherm

The TM isotherm is derived from LM isotherm, assuming that energy of adsorption decreases with surface coverage, resulting from repulsive forces acting on the surface (Temkin 1940). The linear form of isotherm equation can be represented as:

$$qe = (B) \ln A_T + (B) \ln C_e \quad \text{where } B = \frac{RT}{b_T} \tag{13}$$

b (J/mol) where corresponds to TM isotherm constant, T(K) is absolute temperature, and R (J/mol-K) is the universal gas constant. B is a dimensionless constant associated with the heat of adsorption. A_T (L/µg) is adsorption constant related to the binding energy. The TM isotherm plot for Fe-AIB and Fe-AIL is presented in Fig. 14, and the parameters of isotherm are listed in Table 6. The value B for Fe-AIB is 8.7199 and for Fe-AIL is 5.7896. The range of binding energy for the mechanism of ion exchange is 8–16 kj/mol. The low value of binding energy in case of Fe-AIL suggests weak interaction between the solute and adsorbent, and the probable mechanism could be ion exchange. The comparative low value of R^2 for both the adsorbents infers that As (V) adsorption does not closely follow TM isotherm.

D–RM Isotherm

The D–RM isotherm is more general in nature than LM as there is no assumption of homogenous surface or constant potential of adsorption. The linear form of D–RM Isotherm is expressed as:

$$\ln q_e = \ln q_{\max} - \frac{1}{2E^2} \left\{ RT \ln \left(1 + \frac{1}{c_e} \right) \right\}^2 \tag{14}$$

where E (kJ/mol) represents mean adsorption energy. Other parameters of Eq. (14) are the same as discussed in earlier equations. If the E value for adsorption lies in the range 8–16, chemisorption is dominating phenomenon. For E values less than 8, physio-sorption dominates (Wu et al. 2012). The E value for Fe-AIB is greater than 8, and it corresponds to chemisorption. For Fe-AIL, E value is less than 8 which indicates physical adsorption and suggests that sorption process onto the surface of Fe-AIL may not be only ion exchange mechanism or chemisorption. Thus for adsorption of As (V) by Fe-AIL, pore filling can also be a feasible process.

Thermodynamic assessments

The thermodynamic analysis is used to determine the spontaneity of the process. Also, the analysis reveals endothermic or exothermic nature of the reaction, change in entropy or

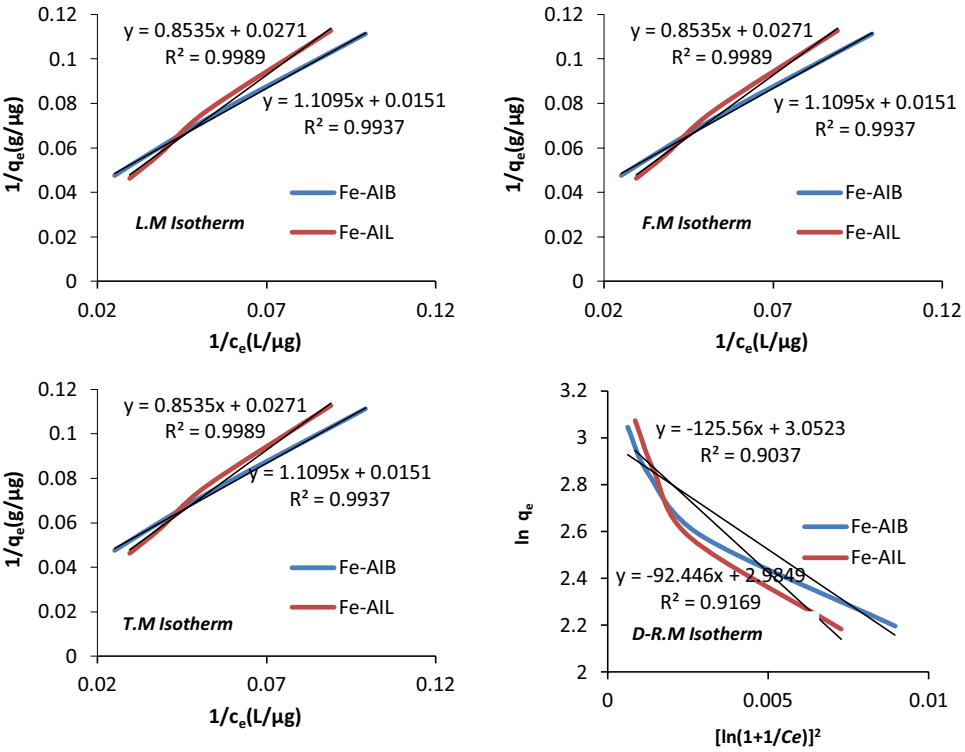

Fig. 14 Four adsorption equilibrium plots: LM isotherm, FM isotherm, TM isotherm, D–RM isotherm. (Experimental conditions: dose, 1 g; contact time, 60 min; pH, 6.0; temperature, 25 °C; agitation speed, 80 rpm)

change in ΔG° (Gibbs free energy) and basis of excitation. Various thermodynamic parameters like ΔH° (enthalpy change), ΔS° (entropy change) and ΔG° can be calculated from the following equations (Balarak et al. 2016):

$$\Delta G^\circ = -\mathrm{RT}\ \ln K_c \tag{15}$$

where K_c is equilibrium thermodynamic constant. Other parameters of Eq. (15) are the same as discussed in earlier equations. The slope and intercept of a linear plot between log K_c and − 1/T from Eq. (16) would yield ΔH° and ΔS°, respectively.

$$\mathrm{Log}\ K_c = \frac{\Delta S^\circ}{2.303R} - \frac{\Delta H^\circ}{2.303\mathrm{RT}} \tag{16}$$

The findings of thermodynamic assessments for adsorption of As (V) on Fe-AIB and Fe-AIL are presented in Table 7. For Fe-AIB, it can be seen from the table that all the values of ΔG° at different temperatures are negative which infers about spontaneous nature of adsorption of As (V) on to Fe-AIB, while the decrement in values of ΔG° with increase in temperature shows that spontaneity increases with increase in temperature (Bulut and Tez 2007). The values of ΔH° and ΔS° are 34.6891 kJ mol^{-1} and 13.4454 kJ mol^{-}1 for Fe-AIB. The typical standard value of ΔH° falls in the range 20.9–418.4 kJ/mol for the heat of chemical reactions, so it can be concluded that adsorption with Fe-AIB takes place through chemisorption and nature of the process was endothermic. The positive value of ΔS° confirms the increment of free active sites at the interface of solid–liquid during adsorption. For Fe-AIL, the positive value of ΔG° implies increment in randomness of the process of adsorption. The positive value of ΔH° and ΔS° infers that the nature of adsorbent is endothermic and randomness

Table 7 Thermodynamic parameters for adsorption of As (V) by Fe-AIB and Fe-AIL

Thermodynamics parameters	Temp (K)	Fe-AIB ΔG° (KJ/mol)	Fe-AIL ΔG° (KJ/mol)
Standard Gibb's free energy	298	− 2.6326	6.9815
	308	− 2.7318	6.3114
	318	− 2.7511	5.9887
	328	− 2.7888	5.7719
	338	− 2.7891	5.7413
Standard enthalpy change	ΔH° (kJ mol^{-1})	34.6891	1.1918
Standard entropy change	ΔS° (kJ mol K^{-1})	13.4454	7.0912

of the process increases with temperature (Bazrafshan et al. 2015).

Effect of co-existing ions

Arsenic-contaminated groundwater might also contain various anions that can hamper the process of adsorption and can be competitor for As (V) ions for adsorption. Phosphate (PO_4^{3-}), sulphate (SO_4^{2-}), silicate (SiO_3^{2-}) and nitrate (NO_3^-) are the major co-existing ions with arsenic, which has the potential to inhabit its adsorption. For understanding the influence of co-existing ions on the removal of arsenate, solution of As (V) was spiked with PO_4^{3-}, SO_4^{2-} and NO_3^- and As (V) removal was determined. At a constant pH 6, phosphate and silicate ions cause the most significant depression in removal percentage of As (V), for both the adsorbents as shown in Fig. 15. The most massive reduction in percentage removal is observed due to the presence of phosphate ions and then by silicate ions under experimental conditions. It is majorly these two anions which compete with As (V) species to be adsorbed by Fe-AIB and Fe-AIL. Due to inner core complexation, PO_4^{3-} and SiO_3^{2-} get strongly adsorbed by surface of Fe oxide. PO_4^{3-} adsorbs Fe oxide when complex on the surface is formed with surface R-OH group (Goldberg 1985).

On the other hand, nitrate and sulphate ions have minimal impact on per cent removal of As (V). SO_4^{2-} and NO_3^-can get adsorb on to the surface by complexation of the outer and inner surface. Also their binding ability with metal oxides is poor as in comparison with As (V) (Meng et al. 2000). Hence, the adsorption of As (V) was significantly influenced by phosphate and silicate ions.

Desorption and regeneration capacity

Reusability of adsorbent with good adsorption capacity, without losing its inherent characteristics, is essential from economic perspective. For a big-scale application or industrial use, it is crucial to make repetitive use of the active sites of the worn adsorbent. This will not only cut down the cost of operation but also will deteriorate the risk of the secondary pollutant. Significant performance for adsorption as well as for desorption is the essential characteristics of an efficient adsorbent. Different types of eluents were used in the past for the evaluation of adsorption–desorption characteristics. In the present study, NaOH solutions of different strengths were used to analyse desorption performance, and their influence on desorption of is presented in Fig. 16. The use of NaOH solution for desorption of As(V) was based on anticipation that the probability of OH- ions to compete with already adsorbed As (V) on Fe-AIB and Fe-AIL. Strong alkalis much supports the desorption of As (V) ions. It can be seen from Fig. 16 that with increase in strength of sodium hydroxide solution, the percentage desorption keeps on increasing for both the adsorbents. 49.1% of adsorbed arsenate ion from Fe-AIB desorbs when 0.02 M sodium hydroxide solution was used. The value goes up to 71.3% when the concentration of sodium hydroxide solution was 0.1 M. Concerning Fe-AIL, high removal percentage (up to 88.78) was achieved at higher concentration (0.1 M). Both Fe-AIB and Fe-AIL are subjected to analysis for reusability as shown in Fig. 17. For Fe-AIB, appreciable decrement is observed after 5 cycles, while in Fe-AIL, the trend of decrements starts after third cycle only.

Adsorption capacity comparison of different adsorbents from the literature for removal of As (V)

The adsorption potential of Fe-AIB and Fe-AIL needs to be compared with other adsorbents used for the same purpose to justify their validity. The value of q_{max} at different operating conditions is listed in Table 8. It is not possible to compare the adsorption capacity of Fe-AIB and Fe-AIL directly with other adsorbents due to different operating conditions.

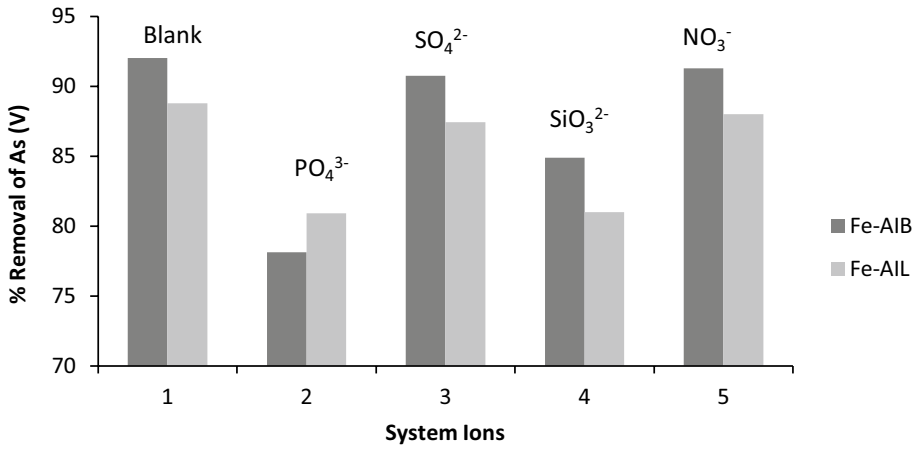

Fig. 15 Effect of co-existing ions on the adsorption of As(V). (Experiment conditions: initial As(V) concentration 100 µg/L, adsorbent dosage 1.0 g/L, solution pH 6.0, agitation speed 60 rpm)

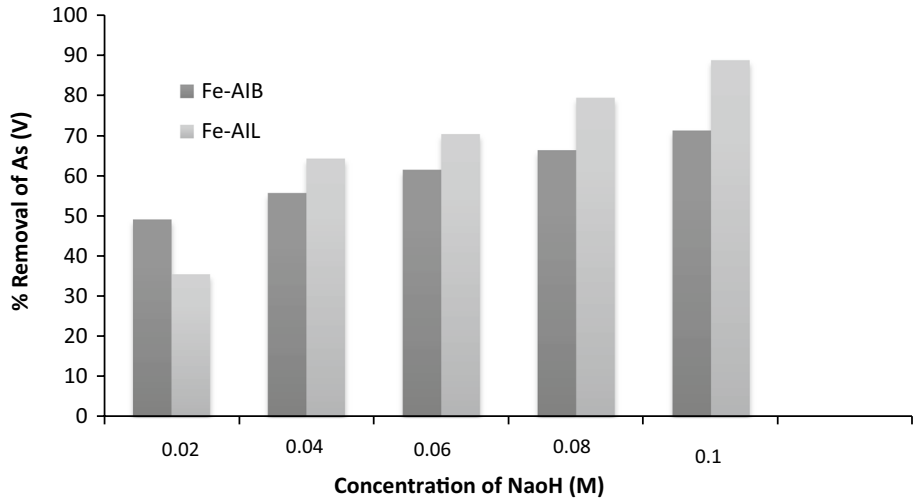

Fig. 16 desorption study on Fe-AIB and Fe-AIL by NaoH as desorbing agent

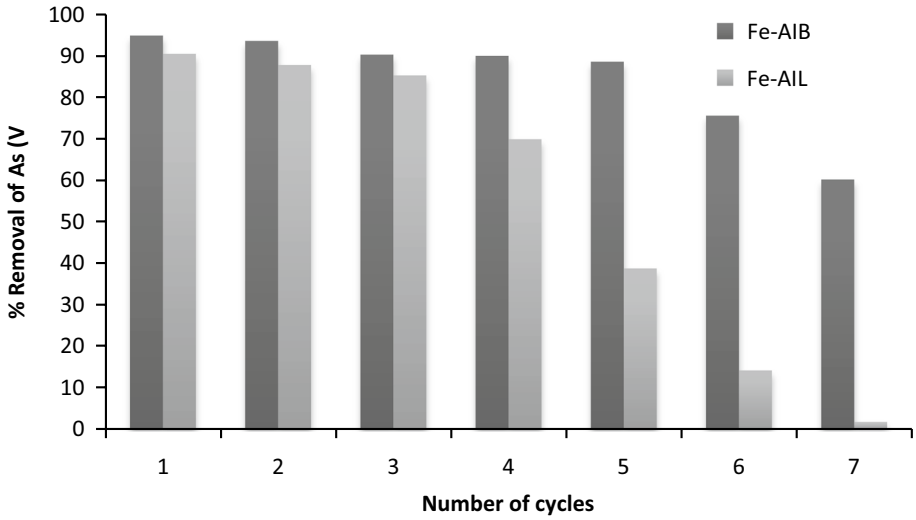

Fig. 17 Variation in percentage removal of As(VI) by repetitive use of Fe-AIB and Fe-AIL

Table 8 Comparison of adsorption capacity of various adsorbent adsorbents used for As (V) remediation

Adsorbent	Initial pH	T (K)	Dose (g/L)	Conc. (mg/L)	q_{max} (mg/g)	References
Manganese oxide loaded sand	4.5	298	2.00	1–100	0.09	Chang et al. (2009)
Laterite (Raw)	5.5	302	20.0	0.2–20	0.51	Maiti et al. (2008)
Coal mine drainage sludge coated polyurethane	6.0	298	1.0	1–100	7.3	Kumar et al. (2020)
Fe-Hickory biochar	5.8	298	1.0	0.1–55	16.0	Hu et al. (2015)
$FeCl_3$ treated lemon residues	6.5	298	0.1	1–100	0.474	Marín-Rangel et al. (2012)
Waste Fe–Mn oxides embedded in chitosan	6.0–6.5	298	1.0	100	26.80	Ociński and Mazur (2020)
Amino-functionalized γFe_2O_3-β-Zeolite	5.0	353	10	5–50	30	Faalzadeh and Faghihian (2015)
Thioglycolated sugarcane carbon	6.0	303	1.0	15	0.085	Roy et al. (2013)
Fe-AIB	6.0	298	1.0	0.1–0.3	0.365	Present study
Fe-AIL	4.9	298	1.0	0.1–0.3	0.298	Present study

However, both the adsorbents used in the present study show good adsorption capacity when compared with other adsorbents. The variation in adsorption capacity for different adsorbents is due to difference in individual properties (functional group, surface structure and available surface area) of adsorbents (Ozsoy and Kumbur 2006).

Conclusion

The present study shows that macro- and microparticles synthesized from the *Azadirachta indica* tree, like Fe-AIL and Fe-AIB, can be used as efficient adsorbent for the remediation of As (V)-contaminated wastewater. It has been observed that various process parameters like pH, adsorbent dose, contact time, initial arsenate concentration, operating temperature and stirring rate affect the process of adsorption. Adsorption studies under different experimental conditions indicate rapid adsorption of As (V) in the first 45 min for Fe-AIB and 30 min for Fe-AIL, thereafter it slowly increases to attain equilibrium in about one hour. The maximum removal of As (V) was noted at 6.0 pH using Fe-AIB and at 4.0 with Fe-AIL. The removal percentage of As (V) from aqueous solution by Fe-AIB was 96.5% (36.5 µg/g) and 90.3% for Fe-AIL. In the analysed range of concentration, the equilibrium data were very well fitted to Langmuir (LM), Freundlich (FM), Temkin isotherm (TM) and reasonably will be fitted to Dubinin–Radushkevich (D–RM) isotherm. The arsenate adsorption kinetics onto Fe-AIB and Fe-AIL follows second-order equation. Different thermodynamic parameters including ΔG°, ΔS° and ΔH° were calculated by using adsorption isotherm data at various temperatures. For Fe-AIB, negative values of ΔG° imply spontaneous adsorption and positive value of ΔG° for Fe-AIL indicates the endothermic nature of its interaction with As (V) ions for adsorption. The efficacy is evaluated in terms of reusability. By analysing adsorption/desorption trends of Fe-AIB and Fe-AIL, we can conclude that Fe-AIB is more suitable than Fe-AIL for continuous flow operation. A consistent high efficiency of approximately 90 per cent after the repeated operation even after five cycles reflects high regeneration capacity of Fe-AIB.

Acknowledgments The authors would like to thank Post-Graduation Research Laboratory, IIT Kanpur, for providing assistance with SEM, XRD, BET and FTIR analysis.

Funding The authors(s) received no specific funding for this work.

Compliance with ethical standards

Conflict of interest The authors declare that they have no conflict of interest.

References

Ahsan H et al (2000) Associations between drinking water and urinary arsenic levels and skin lesions in Bangladesh. J Occup Environ Med 42(12):1195–1201

Albores A et al (1996) Enhanced arsenite-induced hepatic morphological and biochemical changes in phenobarbital-pretreated rats. Toxicol Pathol 24(2):172–180

Ali S et al (2020) High sorption efficiency for As (III) and As (V) from aqueous solutions using novel almond shell biochar. Chemosphere 243:125330

Ansari R, Sadegh M (2007) Application of activated carbon for removal of arsenic ions from aqueous solutions. J Chem 4(1):103–108

Asere T et al (2017) Removal of arsenic (V) from aqueous solutions using chitosan–red scoria and chitosan–pumice blends. Int J Environ Res Public Health 14(8):895

Asere TG, Stevens CV, Du Laing G (2019) Use of (modified) natural adsorbents for arsenic remediation: a review. Sci Total Environ 676:706–720

Balarak D et al (2016) Kinetic, isotherms and thermodynamic modeling for adsorption of acid blue 92 (ab92) from aqueous solution by modified azolla filicoloides. Fresenius Environ Bull 25(5):1322–1331

Baris D et al (2016) Elevated bladder cancer in Northern New England: the role of drinking water and arsenic. JNCI: J Natl Cancer Inst 108(9):1–9

Bayramoglu G et al (2009) Biosorption of phenol and 2-chlorophenol by *Funalia trogii* pellets. Biores Technol 100(10):2685–2691

Bazarafshan E (2017) Efficiency of combined processes of coagulation and modified activated bentonite with sodium hydroxide as a biosorbent in the final treatment of leachate: kinetics and thermodynamics. J Health Res Commun 3(3):58–69

Bazrafshan E et al (2015) Equilibrium and thermodynamics studies for decolorization of reactive black 5 (RB5) by adsorption onto MWCNTs. Desal Water Treat 54(8):2241–2251

Bhattacharya A, Mandal S, Das S (2006) Adsorption of Zn (II) from aqueous solution by using different adsorbents. Chem Eng J 123(1–2):43–51

Bhattacharya A et al (2008) Adsorption, kinetics and equilibrium studies on removal of Cr(VI) from aqueous solutions using different low-cost adsorbents. Chem Eng J 137(3):529–541

Bhaumik R et al (2011) Predicting iron adsorption capacity and thermodynamics onto calcareous soil from aqueous solution by linear regression and neural network modeling. Univ J Environ Res Technol 1(4):486–499

Boddu VM et al (2008) Removal of arsenic (III) and arsenic (V) from aqueous medium using chitosan-coated biosorbent. Water Res 42(3):633–642

Božić D et al (2009) Adsorption of heavy metal ions by sawdust of deciduous trees. J Hazard Mater 171(1–3):684–692

Bulut Y, Tez Z (2007) Adsorption studies on ground shells of hazelnut and almond. J Hazard Mater 149(1):35–41
Bulut Y, Gözübenli N, Aydın H (2007) Equilibrium and kinetics studies for adsorption of direct blue 71 from aqueous solution by wheat shells. J Hazard Mater 144(1–2):300–306
Chang Y-Y, Lee S-M, Yang J-K (2009) Removal of As (III) and As (V) by natural and synthetic metal oxides. Colloids Surf A 346(1–3):202–207
Chen C-L et al (2004) Ingested arsenic, cigarette smoking, and lung cancer risk: a follow-up study in arseniasis-endemic areas in Taiwan. JAMA 292(24):2984–2990
Chen T et al (2020) Synthesis and characterization of a novel magnetic calcium-rich nanocomposite and its remediation behaviour for As (III) and Pb(II) co-contamination in aqueous systems. Sci Total Environ 706:135122
Chiban M et al (2016) Equilibrium and thermodynamic studies for the removal of As (V) ions from aqueous solution using dried plants as adsorbents. Arab J Chem 9:S988–S999
Chien S, Clayton W (1980) Application of Elovich equation to the kinetics of phosphate release and sorption in soils 1. Soil Sci Soc Am J 44(2):265–268
Choudhury TR et al (2014) Arsenic (III) removal from real-life groundwater by adsorption on neem bark (*Azadirachta indica*). Int Res J Pure Appl Chem 4:594–604
Cui J et al (2019) Oxidation and removal of As (III) from soil using novel magnetic nanocomposite derived from biomass waste. Environ Sci: Nano 6(2):478–488
Cullen W, Reimer K (1989) Arsenic speciation in the environment. Chem Rev 89:713–764
Depci T, Kul AR, Önal Y (2012) Competitive adsorption of lead and zinc from aqueous solution on activated carbon prepared from Van apple pulp: study in single- and multi-solute systems. Chem Eng J 200–202:224–236
El Saliby I et al (2013) Adsorption and photocatalytic degradation of methylene blue over hydrogen–titanate nanofibres produced by a peroxide method. Water Res 47(12):4115–4125
Faalzadeh M, Faghihian H (2015) Separation of arsenic from aqueous solutions by amino-functionalized γ-Fe_2O_3-β-zeolite. Sep Sci Technol 50(7):958–964
Ferreccio C et al (2013) Case-control study of arsenic in drinking water and kidney cancer in uniquely exposed Northern Chile. Am J Epidemiol 178(5):813–818
Freundlich H (1906) Stoechiometrie und Verwandtschaftslehre. Zeitschriftfuer Physikalische Chemie 57:385–470
Gnanasangeetha D, SaralaThambavani D (2015) Modelling of As^{3+} adsorption from aqueous solution using *Azadirachta indica* by artificial neural network. Desalin Water Treat 56(7):1839–1854
Goldberg S (1985) Chemical modeling of anion competition on goethite using the constant capacitance model. Soil Sci Soc Am J 49(4):851–856
Hao L et al (2018) A critical review on arsenic removal from water using iron-based adsorbents. RSC Adv 8(69):39545–39560
Hare V et al (2019) Arsenic toxicity and its remediation strategies for fighting the environmental threat. In: Bharagava RN, Chowdhary P (eds) Emerging and eco-friendly approaches for waste management. Springer, Berlin, pp 143–170
Hu X et al (2015) Batch and column sorption of arsenic onto iron-impregnated biochar synthesized through hydrolysis. Water Res 68:206–216
Jadhav AH et al (2015) Preparation, characterization, and kinetic study of end opened carbon nanotubes incorporated polyacrylonitrile electrospun nanofibers for the adsorption of pyrene from aqueous solution. Chem Eng J 259:348–356
Juang R-S, Chen M-L (1997) Application of the Elovich equation to the kinetics of metal sorption with solvent-impregnated resins. Ind Eng Chem Res 36(3):813–820
Kalaruban M et al (2019) Iron-impregnated granular activated carbon for arsenic removal: application to practical column filters. J Environ Manag 239:235–243
Kanwal F et al (2012) Isothermal and thermodynamical modeling of chromium (III) adsorption by composites of polyaniline with rice husk and saw dust. J Chil Chem Soc 57(1):1058–1063
Kumar R et al (2020) Waste sludge derived adsorbents for arsenate removal from water. Chemosphere 239:124832
Kumari P et al (2005) Arsenic removal from the aqueous system using plant biomass: a bioremedial approach. J Ind Microbiol Biotechnol 32(11–12):521–526
Kwok RK, Kaufmann RB, Jakariya M (2006) Arsenic in drinking-water and reproductive health outcomes: a study of participants in the Bangladesh integrated nutrition programme. J Health Popul Nutr 24:190–205
Langmuir I (1918) The adsorption of gases on plane surfaces of glass, mica and platinum. J Am Chem Soc 40(9):1361–1403
Liu J et al (2014) ZnCl2 activated electrospun carbon nanofiber for capacitive desalination. Desalination 344:446–453
Lyu H et al (2020) Biochar/iron (BC/Fe) composites for soil and groundwater remediation: synthesis, applications, and mechanisms. Chemosphere 246:125609
Maiti A et al (2008) Batch and column study: adsorption of arsenate using untreated laterite as adsorbent. Ind Eng Chem Res 47(5):1620–1629
Mandal BK, Suzuki KT (2002) Arsenic round the world: a review. Talanta 58(1):201–235
Marín-Rangel VM et al (2012) As (V) biosorption in an aqueous solution using chemically treated lemon (*Citrus aurantifolia* swingle) residues. J Food Sci 77(1):T10–T14
Meng X, Bang S, Korfiatis GP (2000) Effects of silicate, sulfate, and carbonate on arsenic removal by ferric chloride. Water Res 34(4):1255–1261
Mondal NK et al (2012) Studies on defluoridation of water by tea ash: an unconventional biosorbent. Chem Sci Trans 1(2):239–256
Naeem S et al (2016) Sorption properties of iron impregnated activated carbon web for removal of methylene blue from aqueous media. Fibers Polym 17:1245–1255
Nandi BK, Goswami A, Purkait MK (2009) Adsorption characteristics of brilliant green dye on kaolin. J Hazard Mater 161(1):387–395
Nicomel N et al (2016) Technologies for arsenic removal from water: current status and future perspectives. Int J Environ Res Public Health 13(1):62
Ociński D, Mazur P (2020) Highly efficient arsenic sorbent based on residual from water deironing–Sorption mechanisms and column studies. J Hazard Mater 382:121062
Ozsoy HD, Kumbur H (2006) Adsorption of Cu (II) ions on cotton boll. J Hazard Mater 136(3):911–916
Rajesh KR et al (2010) Equilibrium and kinetic studies on sorption of malachite green using *Hydrilla verticillata* biomass
Rango T et al (2013) Mobilization of arsenic and other naturally occurring contaminants in groundwater of the Main Ethiopian Rift aquifers. Water Res 47(15):5801–5818
Ranjan A (2019) Spatial analysis of arsenic contamination of groundwater around the world and India
Ravikovitch PI, Neimark AV (2006) Density functional theory model of adsorption on amorphous and microporous silica materials. Langmuir 22(26):11171–11179
Rossman TG, Uddin AN, Burns FJ (2004) Evidence that arsenite acts as a cocarcinogen in skin cancer. Toxicol Appl Pharmacol 198(3):394–404
Roy P et al (2013) Removal of arsenic (III) and arsenic (V) on chemically modified low-cost adsorbent: batch and column operations. Appl Water Sci 3(1):293–309

Roy P, Mondal N, Das K (2014) Modeling of the adsorptive removal of arsenic: a statistical approach. J Environ Chem Eng 2(1):585–597
Roy P et al (2017) Modeling of the adsorptive removal of arsenic (III) using plant biomass: a bioremedial approach. Appl Water Sci 7(3):1307–1321
Ryu S-R et al (2017) Adsorption of As (III) and As (V) in groundwater by Fe–Mn binary oxide-impregnated granular activated carbon (IMIGAC). J Taiwan Inst Chem Eng 72:62–69
Sarı A, Tuzen M (2010) Biosorption of As (III) and As (V) from aqueous solution by lichen (*Xanthoria parietina*) biomass. Sep Sci Technol 45(4):463–471
Shah I et al (2015) Iron impregnated activated carbon as an efficient adsorbent for the removal of methylene blue: regeneration and kinetics studies. PLoS ONE 10(4):e0122603
Shankar S, Shanker U, Shikha (2014) Arsenic contamination of groundwater: a review of sources, prevalence, health risks, and strategies for mitigation. Sci World J 2014:304524
Singh TS, Pant K (2004) Equilibrium, kinetics and thermodynamic studies for adsorption of As (III) on activated alumina. Sep Purif Technol 36(2):139–147
Smeester L, Fry RC (2018) Long-term health effects and underlying biological mechanisms of developmental exposure to arsenic. Curr Environ Health Rep 5(1):134–144
Smith AH et al (2006) Increased mortality from lung cancer and bronchiectasis in young adults after exposure to arsenic in utero and in early childhood. Environ Health Perspect 114(8):1293–1296
Srivastava R, Rupainwar DC (2011) A comparative evaluation for adsorption of dye on Neem bark and mango bark powder. Indian J Chem Technol 18:67–75
Taştan BE, Duygu E, Dönmez G (2012) Boron bioremoval by a newly isolated *Chlorella* sp. and its stimulation by growth stimulators. Water Res 46(1):167–175
Tchounwou P et al (2015) Arsenic and cancer, handbook of arsenic toxicology. Elsevier Inc., Amsterdam
Tchounwou PB et al (2019) State of the science review of the health effects of inorganic arsenic: perspectives for future research. Environ Toxicol 34(2):188–202
Temkin M (1940) Kinetics of ammonia synthesis on promoted iron catalysts. Acta physiochim. URSS 12:327–356
Thapa S, Pokhrel MR (2012) Removal of as (III) from aqueous solution using Fe(III) loaded pomegranate waste. J Nepal Chem Soc 30:29–36
Tiwari D et al (1999) Biosorptive behaviour of Mango (*Mangifera indica*) and Neem (*Azadirachta indica*) bark for Hg^{2+}, Cr^{3+} and Cd^{2+} toxic ions from aqueous solutions: a radiotracer study. Appl Radiat Isot 50(4):631–642
Tripathy SS, Raichur AM (2008) Enhanced adsorption capacity of activated alumina by impregnation with alum for removal of As (V) from water. Chem Eng J 138(1–3):179–186
Tsai S-Y et al (2003) The effects of chronic arsenic exposure from drinking water on the neurobehavioral development in adolescence. Neurotoxicology 24(4–5):747–753
Tseng C-H (2009) A review on environmental factors regulating arsenic methylation in humans. Toxicol Appl Pharmacol 235(3):338–350
Tseng C-H et al (2000) Long-term arsenic exposure and incidence of non-insulin-dependent diabetes mellitus: a cohort study in arseniasis-hyperendemic villages in Taiwan. Environ Health Perspect 108(9):847–851
Upadhyay MK et al (2019) An assessment of arsenic hazard in groundwater–soil–rice system in two villages of Nadia district, West Bengal, India. Environ Geochem Health 41:1–15
Verma L et al (2019) As (III) and As (V) removal by using iron impregnated biosorbents derived from waste biomass of *Citrus limmeta* (peel and pulp) from the aqueous solution and ground water. J Environ Manag 250:109452
Wasserman GA et al (2004) Water arsenic exposure and children's intellectual function in Araihazar, Bangladesh. Environ Health Perspect 112(13):1329–1333
Wu Y et al (2012) The characteristics of waste Saccharomyces cerevisiae biosorption of arsenic (III). Environ Sci Pollut Res 19(8):3371–3379
Yadav SK, Singh DK, Sinha S (2014) Chemical carbonization of papaya seed originated charcoals for sorption of Pb(II) from aqueous solution. J Environ Chem Eng 2(1):9–19
Yakun H et al (2011) Fluoride removal by lanthanum alginate bead: adsorbent characterization and adsorption mechanism. Chin J Chem Eng 19(3):365–370
Zeng H et al (2020) Arsenic (V) removal by granular adsorbents made from water treatment residuals materials and chitosan. Colloids Surf A 585:124036
Zhu S et al (2020) Goethite modified biochar as a multifunctional amendment for cationic Cd (II), anionic As (III), roxarsone, and phosphorus in soil and water. J Clean Prod 247:119579